

Fusion of $^{16}\text{O} + ^{148,150,152,154}\text{Sm}$ at sub-barrier energies

R. G. Stokstad

*Oak Ridge National Laboratory, Oak Ridge, Tennessee 37830
and The Weizmann Institute of Science, Rehovot, Israel*

Y. Eisen, S. Kaplanis, D. Pelte, U. Smilansky, and I. Tserruya

The Weizmann Institute of Science, Rehovot, Israel

(Received 19 November 1979)

Measurements of the cross section for fusion of ^{16}O with $^{148,150,152,154}\text{Sm}$ have been made in the range $60 \leq E_{^{16}\text{O}} \leq 75$ MeV. Evaporation residues trapped in a carbon catcher foil were observed off line by means of the K x rays emitted by radioactive Yb nuclei and their daughters. Absolute cross sections varying in magnitude from 0.1 to 400 mb were determined with an uncertainty of $\pm 10\%$. The cross sections for individual x - n channels were also determined. At high energies, the fusion cross sections for all isotopes are similar, whereas at lower bombarding energies the cross sections for the more deformed targets are larger than those for the spherical targets.

[NUCLEAR REACTIONS Measured σ_{fusion} for $^{16}\text{O} + ^{148,150,152,154}\text{Sm}$, $E_{^{16}\text{O}}^{\text{lab}} = 60-75$ MeV. Observation of x rays from radioactive evaporation residues.]

I. INTRODUCTION

The study of subtle effects such as nuclear deformation on the cross section for fusion of complex nuclei requires experimental data of high precision at low bombarding energies, where penetrability effects are important.^{1,2} We present here an experimental study of the fusion of ^{16}O with the even-even isotopes of samarium, $^{148,150,152,154}\text{Sm}$, which undergo a transition from a spherical to a deformed equilibrium shape as the neutron number increases. This report considers the experimental techniques and methods of analysis leading to values of the cross section for fusion. The attainment of high precision is emphasized. The interpretation of these experimental results, as well as a discussion of related experimental and theoretical work, will appear in a subsequent article. A short account of this work has been published.³

II. EXPERIMENTAL CRITERIA

The choice of projectile and targets was governed by three factors. (i) The interpretation of the results is simplified if only one of the colliding nuclei is deformed; thus ^{16}O was chosen as the projectile. (ii) The Sm isotopes offer a variation in nuclear deformation without an accompanying change in atomic number. Thus the relatively large changes in the interaction barrier associated with a change of nuclear charge are eliminated. The equilibrium deformations for these isotopes are well known.⁴ (iii) The isotopes of

Yb formed by the fusion of $^{16}\text{O} + \text{Sm}$ at energies below 70 MeV c.m. should have a negligible fission width.⁵ The entire fusion cross section is thus concentrated in the yield of evaporation residues.

A number of direct experimental methods can be used to measure the cross section for production of evaporation residues. These include direct identification by $\Delta E - E$ energy loss,⁶ time of flight,⁷ and track detectors.⁸ Of these three methods, the first is unsuitable because the energy of the Yb compound nuclei (≈ 7 MeV) is too low. Both the first and the second methods require measurement and integration of an angular distribution which is strongly forward peaked. The residues must be detected in the presence of intense elastic scattering. The third method would not easily distinguish evaporation residues ($A \sim 170$) from elastically scattered or Coulomb-excited target recoils ($A \sim 154$).

Indirect methods involve the detection of some characteristic radiation emitted by the evaporation residue along its path back to the valley of stability. In-beam measurements of discrete γ -ray transitions following x - n reactions are effective at higher energies⁹ but have a poor signal-to-noise ratio at low bombarding energies because of Coulomb excitation of the target and reactions with light contaminants, e.g., ^{12}C , ^{16}O , in the target. The detection of delayed γ rays from the radioactive nuclei formed following prompt neutron emission improves the signal-to-noise ratio, but requires (in addition to an unstable residue) an absolute normalization for the intensity of transitions in the decay scheme,

i.e., the number of transitions per 100 decays. Such information is often available provided a detailed study of γ -ray and conversion electron spectra has been made.

The detection of delayed x-ray emission offers the highest signal-to-noise ratio of all the techniques which we considered. Because proton rich nuclei in the rare earth region decay predominantly by electron capture, and because there are many highly converted electromagnetic transitions, the yield of x rays per decay often exceeds unity, whereas for a given γ ray this yield is usually substantially smaller. As is the case with delayed γ rays, a knowledge of the absolute intensity of x-ray emission per decay is required. However, the large and rather regular contribution by electron capture to the number of K vacancies tends to reduce the relative uncertainty in the total intensity. A disadvantage, however, is that isotopic identification of a residue no longer follows directly from the energy of the radiation, but is only possible through an analysis of the time dependence of the decay.

We chose the detection of x rays for the present experiments primarily because it would enable us to measure small cross sections at the low bombarding energies where the relative effects of nuclear deformation are expected to be largest.

III. THE EXPERIMENTAL CONFIGURATION AND PROCEDURE

The essential features of the experiment are centered around the collection of the evaporation residues in a catcher foil and the subsequent off-line measurement of the x rays. Beams of ^{16}O produced by the 14-UD Pelletron accelerator at the Weizmann Institute were used to bombard thin, isotopically enriched targets of Sm. The catcher foil, made of carbon, was located approximately 2 mm behind the target. The beam emerged from the target and catcher foil and was stopped in a magnetically suppressed Faraday cup. Two surface barrier detectors were used to monitor the elastic scattering from the target. Following a bombardment of typically one-half to one hour, the catcher foil was removed from the scattering chamber and placed before a Ge spectrometer. X-ray spectra were then recorded at various time intervals until further activity could no longer be detected. We consider in more detail now each of the above elements of the experiment.

A. The ^{16}O beam

Energies between 60 MeV and 75 MeV were used. The energy of the beam was determined by calibrating the 90° analyzing magnet of the

newly operational 14-UD Pelletron with the analyzing magnet associated with the Institute's EN Van de Graaff. This was done by comparing directly in an elastic scattering experiment the energy of beams produced by each of these accelerators. This procedure resulted in an estimated uncertainty of $\pm 0.15\%$ on the absolute energy of the ^{16}O beam.

B. The targets

The targets were prepared by vacuum evaporation of samarium oxide enriched to the following percentage in the main isotope for each of the four targets: (A, %), (148, 95), (150, 95), (152, 98), and (154, 99). The target material was backed by a carbon film having a thickness typically of $20 \mu\text{g}/\text{cm}^2$. The samarium oxide was first mixed with tantalum, and thus was reduced to elemental form during the evaporation. An amount of tantalum varying up to 20% of the total number of target nuclei was deposited on the carbon foil as a result of this procedure, however. This amount was measured for each target by using a surface-barrier detector to observe the relative number of ^{16}O nuclei scattered at 60° from Sm and from Ta. This was an important correction insofar as the elastic scattering from the Ta impurity was not resolved by the surface-barrier detectors during an actual irradiation. In this case, the monitor detectors were at a more forward angle (40°) and viewed the target through the carbon catcher foil. Otherwise, the Ta impurity had no effect on the experiment, since the ^{16}O energy was too low to initiate nuclear reactions.

The thicknesses of the targets varied between 100 and $200 \mu\text{g}/\text{cm}^2$ and were determined using the measured elastic scattering, the integrated charge at the Faraday cup, and the known Rutherford cross section. These measurements of the target thickness also showed that no detectable amount of Sm was lost from the target, even at the highest beam intensities. The target thickness thus determined had an uncertainty of about 5% and was used only for estimating the energy loss of the beam in the target; it did not enter directly into the determination of the cross section (see Sec. IIID below).

C. The catcher foils

Carbon, rather than aluminum, was chosen as the material for the catcher foil since the compound nuclei formed in the reaction of $^{16}\text{O} + ^{12}\text{C}$ have a high velocity and are not stopped in the catcher foil. It is this fact which is largely responsible for the low background and resulting high sensitivity of this measurement. Individual carbon foils of thickness $\sim 250 \mu\text{g}/\text{cm}^2$ were pre-

pared by vacuum evaporation. Three to four of these foils were then combined on a single target frame to form a catcher foil. A thin film of organic material, amyl acetate, was used between each carbon foil as a clamping agent. Foils so made varied in thickness from 700 to 1000 $\mu\text{g}/\text{cm}^2$. Upon a first exposure to an intense beam, some of the foils "exploded," presumably because of the presence of the organic film sandwiched between the carbon foils. Those foils which were not damaged initially (raising the beam current gradually increased the survival rate) were able to withstand particle-current densities of up to ~ 30 nA/mm^2 with no deterioration. Attempts to detect activity remaining in the target and in an additional carbon foil placed behind the catcher foil demonstrated that all of the evaporation residues were indeed stopped in the catcher foil. Measurements made with varying beam intensities showed that activity was not lost from the catcher foil because of beam heating.

The catcher foils developed a dimple where the beam intersected the foil. The effective displacement of the foil due to this dimple was measured for each foil with a microscope and was used to correct the efficiency for the detection of x rays from each catcher foil. The magnitude of this correction was usually less than 4%.

D. The monitor system

Surface-barrier detectors placed at $\pm 40^\circ$ and at 25 cm distance from the target were used to monitor the scattering from the Sm. These events (elastic scattering plus Coulomb excitation) were well resolved from reaction products produced by light contaminants in the target (carbon and oxygen) and by the carbon catcher foil. Since the solid angle of these detectors and the scattering angle could be measured with high precision, and since the sum of the scattered particles in the two detectors was insensitive to small variations in the angle of the beam with respect to the chamber axis, an absolute measure of the product of the time-integrated number of beam particles and target atoms could be obtained with high precision. Checks using (i) optical model calculations and (ii) the measured ratio of the elastic scattering at 40° and 60° showed that the summed cross section for elastic and inelastic scattering at 40° is given by the Rutherford formula to within $\pm 0.2\%$ and 0.7% , respectively. The accuracy of the above techniques is estimated at 1% for systematic errors and 2% for random errors. The random errors were estimated by an analysis of runs at different energies using the same target.

The intensity of the beam as a function of time

during the irradiation was recorded by multi-scaling, in one-minute intervals, the number of elastic events in the monitor counters.

E. The Ge spectrometer

The x-ray detector¹⁰ consisted of 1.5 cm^3 of intrinsically pure Ge and employed an optically coupled feed-back loop in the preamplifier. A resolution of 350 eV (FWHM) was obtained at 50 keV. The catcher foil was positioned in front of the detector such that the photopeak efficiency in the range of 30–60 keV was 5.5%. This efficiency was determined using a variety of calibrated point sources (^{241}Am , ^{137}Cs , ^{57}Co , ^{152}Eu) mounted on frames identical to those holding the catcher foil. An empirical function¹¹ was then used to fit these calibration points and to determine the photopeak efficiency at any energy in the range from 20 to 150 keV to an accuracy of $\pm 3\%$. The total efficiency was also measured and used, together with the known decay schemes, to estimate sum corrections for the calibrated sources. The spectrometer was shielded by 10 cm of lead.

IV. ANALYSIS OF THE X-RAY SPECTRA

The x rays and γ rays from the catcher foils were measured in the range from 10–250 keV. The portion of the spectrum including the x rays associated with the decay of Yb, Tm, and Er nuclei is shown in Figs. 1 and 2. Figure 1 presents a spectrum obtained in 5 min of counting just after a 28-min bombardment of ^{150}Sm with 70–

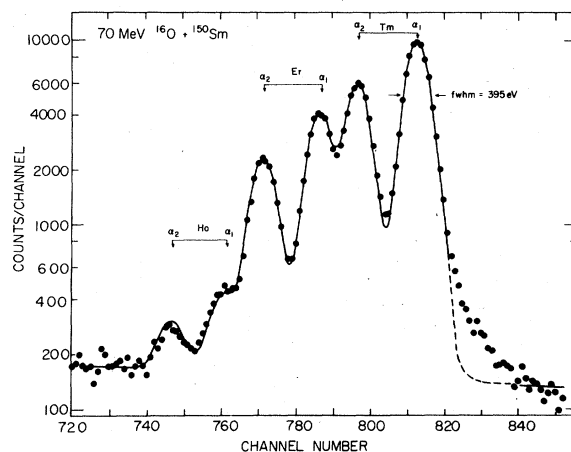


FIG. 1. Photon spectrum covering the range from 45 to 53 keV. The Tm $K_{\alpha 1}$ and $K_{\alpha 2}$ x rays are produced by the electron-capture decay of Yb and subsequent internal conversion in the Tm daughter. The full curve is a fit to the data in which each component is approximated by a Gaussian. The cross section for fusion in this case is 243 mb and the counting interval was 5 min.

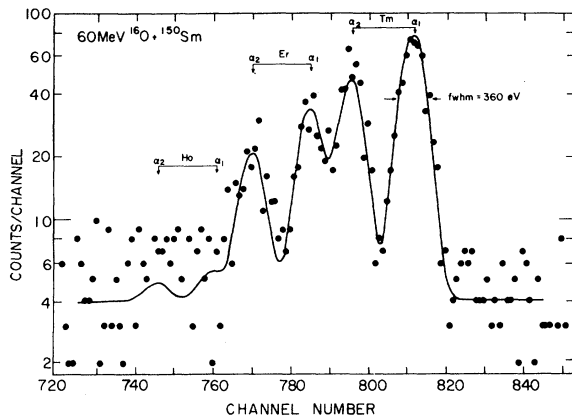


FIG. 2. Same as Fig. 1, except that the bombarding energy is lower and the fusion cross section is only 0.47 mb. The bombardment time was 1 h and the counting interval was 10 mb.

MeV ^{16}O ions. Individual $K_{\alpha 1}$ and $K_{\alpha 2}$ lines from all the decay products are resolved. The full curve is a least-squares fit of Gaussian peak shapes in which the widths, relative energy spacings, and $K_{\alpha 1}/K_{\alpha 2}$ intensity ratios are fixed quantities. The portion of the curve shown as a dashed line indicates a region of data excluded from the fit because of pile-up distortion. (Inclusion of this region has a sizable effect on χ^2 but a negligible effect on the peak areas.)

A spectrum obtained at the lowest bombarding energy, 60 MeV, for which the fusion cross section is much smaller, is shown in Fig. 2. This spectrum was obtained in 10 min of counting after a 45-min bombardment. The signal-to-noise ratio in this case was still high. Thus, the statistical uncertainty in the peak area was a negligible source of error in the determination of the cross section, even at the lowest bombarding energies. In cases where a γ -ray transition occurred in the K x-ray energy region, the γ -ray peak was analyzed simultaneously with the x rays. The K_{β} x rays were not analyzed. Electronic dead time was measured by evaluating the area of a peak from an electronic pulser.

V. DETERMINATION OF THE ABSOLUTE CROSS SECTION

Evaluation of the absolute cross section depends directly on the Rutherford cross section, the number of counts in the monitor, the measured intensity of the x rays, and the absolute intensity, in photons per decay, of the various radioactive products in the catcher foil. All but the last quantity have been discussed so far.

A. Absolute K x-ray intensities

Given a decay scheme with an absolute normalization, it is possible to calculate the number of K vacancies formed per 100 decays. Since the lifetime of a K vacancy ($\sim 10^{-17}$ sec) is short compared to typical nuclear decay times, electron capture and the internal conversion of transitions in a cascade are independent, additive sources of K x rays.

In evaluating the K vacancies produced by electron capture to each level of a daughter nucleus and K vacancies produced subsequently by each individual nuclear transition in the decay scheme, use was made of the quantities f_e/f_t from Ref. 12, ϵ_x/ϵ from Ref. 13, and $\alpha_K/\alpha_{\text{tot}}$ from Ref. 14. The total number of K_{α} x rays was then obtained using the fluorescence yield ω_K and K_{α}/K_{β} intensity ratios from Ref. 13. Decay schemes from the Nuclear Data Sheets¹⁵ were used. In some cases normalized decay schemes were not available from this source but had appeared in the literature subsequent to the last evaluation. An effort was made to use the most recent sources of information. For a number of nuclei with shorter half-lives and located relatively far from stability, an educated guess at the x-ray intensity was necessary. These cases, however, had a rather small influence on the overall determination of the cross section. The results of the above evaluation are given in Table I.

It is difficult to assess an error for each absolute intensity. In the few cases where an error is given in the literature for an absolute normalization, the error is of the order of 10% or less. We have therefore assumed an error of 10% for each intensity unless it is known to be larger. Since a given decay chain has at least two and sometimes up to four members before stability is reached, an internal check on the relative accuracy of the members in a given chain is possible. This check indicates that the choice of 10% for the typical error is a reasonable one.

In one case it was clear, from a lack of internal consistency in fitting the data, that an evaluated absolute intensity was in error. Examination of the decay schemes indicated a probable source of the error and led to a 15% increase in the calculated absolute intensity for the decay of ^{163}Yb . With this modification, internal consistency was obtained and the maximum effect on the deduced cross section was less than 7%.

Since the sources (catcher foils) are used in a high efficiency geometry, corrections for the simultaneous detection of more than one photon (summing) were applied. These were evaluated for each level scheme and were typically 5%, but did not exceed 13%.

TABLE I. Mean lifetimes and K_{α} x-ray intensities (EC denotes electron capture; IC denotes internal conversion).

Parent nucleus	t_m (min)	K vacancies/100 decays		$K_{\alpha 1} + K_{\alpha 2}$ intensity (photons/100 decays)
		EC	IC	
^{159}Yb	2.0 ^a			75 ^a
^{159}Tm	17.3			75 ^a
^{159}Er	51.9			75 ^a
^{159}Ho	47.6	83	76	118
^{160}Yb	6.9			75 ^a
^{160}Tm	13.3	71	23	70
^{160}Er	2474.0	83	17	75
^{160}Ho	36.9	83	18	75
^{161}Yb	6.1	73	25	72 ^b
^{161}Tm	54.8	76	138	159
^{161}Er	280.2	83	17	74
^{161}Ho	216.6	83	17	74
^{162}Yb	27.3	83	8	69 ^c
^{162}Tm	31.3	75	25	74 ^d
^{163}Yb	16.0	73	24	72 ^e
^{163}Tm	156.7	82	55	102
^{163}Er	108.2	84	0	63
^{164}Yb	109.4	84	1	63 ^c
^{164}Tm	2.9	51	9	45 ^c
^{165}Yb	14.3	75	51	94
^{165}Tm	2602.0	84	17	75
^{165}Er	896.8	81	0	60
^{166}Yb	4908.0	73	70	106
^{166}Tm	667.0	83	24	80
^{167}Yb	25.2	84	116	149
^{167}Tm	19195.0	82	21	77

^aThe value is a guess, based on systematics, and is not crucial for this analysis.

^bAssumes the decay of ^{161}Yb is similar to the decay of ^{163}Yb .

^cAn average of an experimental value and the value calculated from the level scheme.

^dAn experimental value.

^eAssumes no appreciable capture to the ground state. The decay scheme assumed 32% capture to the ground state, but this led to an inconsistency in fitting the data.

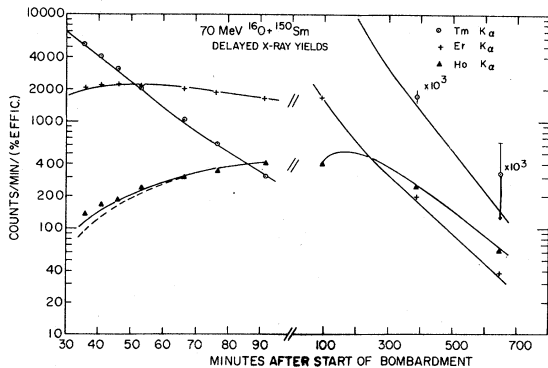


FIG. 3. The x-ray count rate as a function of time. The length of the bombardment was 28 min. The full curves are fits to the data incorporating known half-lives and absolute x-ray intensities.

B. Analysis of the time dependence of the x-ray intensity

Several isotopes, each with a different half-life, can contribute to the intensity of a given x ray. Thus, the time dependence of the intensity is complicated. Figure 3 illustrates a typical case. The growth and decay patterns associated with a parent, daughter, and granddaughter are seen, respectively, in the Tm, Er, and Ho x-ray intensities. Using the known half-lives and absolute x-ray intensities and assuming a parent-daughter relationship, it is possible to determine quite accurately the relative amounts of each isotope. The procedure was to fit all of the experimental data shown in Fig. 3 simultaneously, with the only unknowns being the activity present in each Yb isotope at the end of the bombardment.

The effect of variations in beam intensity during the irradiation and of the variation in source strength during a counting interval were treated exactly in the computer program used to fit the measured time dependence of the x-ray intensities.

Elementary statistical considerations for neutron evaporation usually limited to three the number of mass chains which needed to be included in a fit. Detailed statistical model calculations¹⁶ showed that charged-particle emission is strongly hindered relative to neutron emission for the reactions and bombarding energies studied here. The emission of two protons, which leads to stable isotopes of Er, was predicted to be negligible. Nevertheless, it seems possible in some cases to detect charged-particle emission through a detailed examination of the time dependence of the daughter activities. The fitted yield of Ho x rays is increased from the dashed line to the full line in Fig. 3 by the inclusion of ~1% of $2p-1n$ emission from the compound nucleus. Deduced yields of charged-particle emission were largest for $^{16}\text{O}+^{148}\text{Sm}$, but even in this case did not exceed 15%. The total fusion cross section was independent to within ~1-2% of whether or not the possibility of charged-particle emission was included in the fit.

The full curves in Fig. 3 are the result of a simultaneous fit of all the data shown in the figure. Figures 4 and 5 show the intensities for the parent decay and daughter decay, respectively. The contributions of the various isotopes (labeled by the number of mass units emitted from the compound nucleus) are shown. It may be seen from these two figures how the different half-lives associated with the different isotopes enable a determination of their relative contributions, provided the sources are counted over a sufficiently long time span.

The relative amounts of the various evaporation residues are listed in Table II and presented in

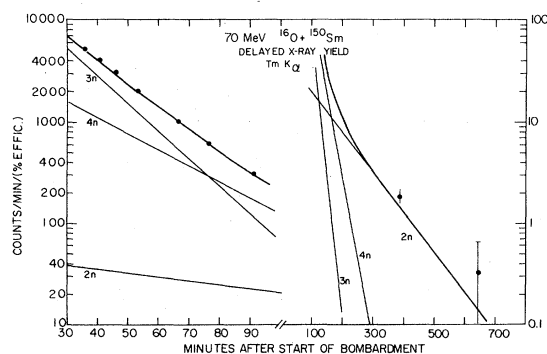


FIG. 4. The time dependence of the parent activity with the deduced contributions of the $2n$, $3n$, and $4n$ activities to the total. Note that measurements at later times effectively determine the $2n$ portion.

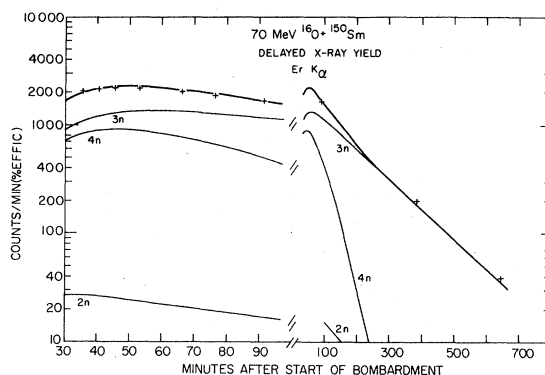


FIG. 5. Same as Fig. 4, but for the daughter activity. In this case the later times determine the $3n$ portion.

TABLE II. $x-n$ distributions (%).

E_{lab}	Target	$1n^a$	$2n$	$3n$	$4n$	$5n$
75.0	148		5(7) ^b	84(4)	11(8)	
	150		2(1)	43(2)	55(2)	
	152			15(2)	81(2)	4(1)
	154				66(2)	34(2)
70.0	148		14(1)	81(2)	5(3)	
	150		2(1)	72(2)	26(1)	
	152			37(1)	62(1)	1(1)
	154			8(1)	82(2)	9(1)
67.5	148		21(1)	78(1)	1(1)	
	150		5(1)	81(1)	14(3)	
	154			18(2)	82(4)	
65.0	148		39(1)	59(1)	2(2)	
	150		8(2)	86(2)	6(2)	
	152		2(1)	73(2)	25(1)	
	154			32(1)	68(2)	
63.75	148	2(2)	49(2)	49(2)		
	150		10(1)	81(2)	9(2)	
	152		1(5)	83(2)	16(1)	
	154			45(2)	55(2)	
62.5	148	3(1)	62(2)	35(2)		
	150		13(2)	80(2)	7(2)	
	152		2(1)	90(3)	8(2)	
	154			51(2)	49(2)	
61.25	148	12(6)	73(4)	15(4)		
	150		16(4)	71(3)	13(1)	
	152		5(2)	92(3)	3(1)	
	154			68(2)	32(5)	
60.0	148	9(5)	91(7)			
	150		24(3)	67(4)	9(4)	
	152		7(3)	93(3)		
	154			80(2)	20(5)	

^aThe value of n denotes the number of atomic mass units evaporated from the compound nucleus. For ^{148}Sm and $E_{\text{lab}} \geq 65$ MeV, charged-particle emission up to ~15% of the total is included. In all other cases, n is the number of neutrons evaporated to a very good approximation.

^bThe number in parentheses is the uncertainty on the last digit.

Fig. 6. The full curves in Fig. 6 are only to guide the eye. The value of n denotes the number of atomic mass units removed from the compound nucleus; since charged-particle emission is small, n approximates the number of neutrons evaporated. The cross section for fusion, which is the sum of the various x - n channels and charged-particle emission is listed in Table III and shown in Fig.

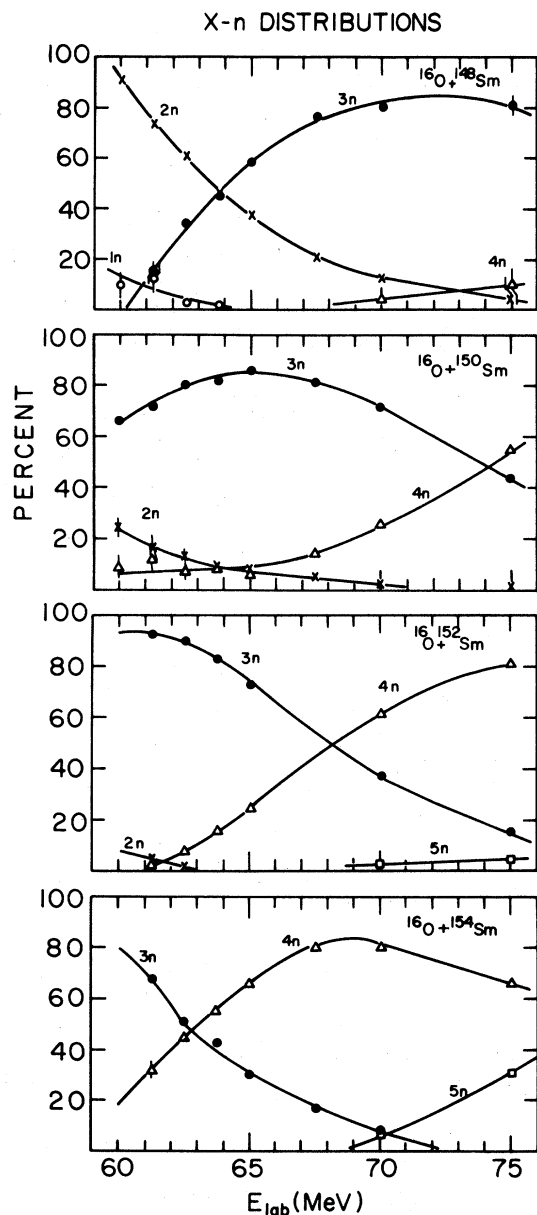


FIG. 6. The distribution of the evaporation residues as a function of bombarding energy for the four systems studied. The value of n denotes the number of mass units evaporated by the compound nucleus. The yields are expressed as a percentage of the total fusion cross section. The lines are only to guide the eye.

7. The laboratory bombarding energies given in Table III correspond to the energy at the center of the target. (The stopping powers of Northcliffe and Schilling¹⁷ were used to estimate the energy loss in the target.) Figure 7 shows that the cross sections obtained for the different isotopes are nearly identical at the highest bombarding energy. As the bombarding energy is reduced, however, σ_{fus} exhibits a systematic variation, with the more deformed isotopes exhibiting progressively larger cross sections relative to the less deformed isotopes. A quantitative analysis of these data in terms of the deformation of the target nucleus will be given in a subsequent paper.

VI. DISCUSSION OF ERRORS

The sources of error in the present experiment can be divided into several categories. Purely systematic errors consist only of the absolute Ge-detector efficiency ($\pm 3\%$) and the solid angle of the monitor detectors ($\pm 1\%$). Purely random errors include the number of counts in the monitor detector and the reproducibility of the monitor system in different runs. Experimental checks show that these contribute an error of $\pm 2\%$ to the cross section. An additional source of random error involves the accuracy of the correction applied to the efficiency of the Ge detector due to variations in the position of the source ($\pm 2\%$).

The large value of χ^2 sometimes obtained from fitting the time decay of the sources indicated that errors other than random errors on the peak areas were present. The main additional source of error most likely was the absolute x-ray intensities. This is indicated by the fact that values of χ^2/N of the order of unity were routinely obtained when only a parent decay or only a daughter decay curve was fit. Nevertheless, a straightforward evaluation of the error on the total fusion cross section for a simultaneous fit of all members of the decay chains, obtained by multiplying the internal error with $(2\chi^2/N)^{1/2}$, yielded errors of typically 2% and never more than 7%.

Sources of error which are partly random and partly systematic in nature include the errors on the absolute x-ray intensities and the corrections for summing of coincidental radiations ($\pm 3\%$). We have assumed that each absolute intensity is known to $\pm 10\%$ and that two independent absolute intensities (a parent and a daughter) contribute to each cross section. Thus a net contribution of $\pm 7\%$ to the total error is associated with the uncertainty in the absolute intensities. This is a conservative estimate since there is often a grand-daughter activity present. Also, more than one mass chain contributes to the x-ray yield, which further randomizes the error from the absolute

TABLE III. Fusion cross sections for $^{16}\text{O} + ^{148,150,152,154}\text{Sm}$.^a

E_{lab} (MeV)	^{148}Sm (mb)	^{150}Sm (mb)	E_{lab} (MeV)	^{152}Sm (mb)	E_{lab} (MeV)	^{154}Sm (mb)
75.02	404.0	440.0	74.95	462.0	75.06	430.0
70.01	183.0	243.0	69.94	213.0	70.05	235.0
67.51	89.4	117.0			67.54	134.0
65.00	27.0	38.4	64.93	43.9	65.04	55.8
63.75	10.7	20.2	63.68	24.4	63.78	29.4
62.49	3.13	7.75	62.42	11.7	62.53	15.3
61.24	0.721	2.22	61.17	4.40	61.28	6.24
59.98	0.115	0.472	59.92	1.06	60.03	2.21

^aThe uncertainty on the fusion cross sections is $\pm 10\%$. The uncertainty on the beam energy is $\pm 0.15\%$.

intensities.

Since the x - n distributions, expressed as a percentage of the fusion cross section, vary slowly with bombarding energy (see Fig. 6) it was possible to extrapolate accurately the relative amounts of $1n$, $2n$, and $3n$ emission at the lowest bombarding energy. Fixing these relative amounts in the fit greatly reduced the error in the cross section at the lowest bombarding energy where a low yield prohibited observing the x rays over a long time interval.

A summation in quadrature of random and partially random errors yields a standard deviation of 8.4%. The corresponding value for purely

systematic errors is 3.2%. If all errors are added in quadrature, a value of 9% is obtained. We have therefore adopted an error of $\pm 10\%$ for each cross section listed in Table III.

The reproducibility of the experimental method was checked by repeating selected measurements on different runs and using different targets and catcher foils. The maximum discrepancy encountered was 5.5%. In one case (70 MeV $^{16}\text{O} + ^{148}\text{Sm}$), the γ rays were analyzed to deduce cross sections for the individual mass chains. These cross sections agreed within a few percent with those deduced from the analysis of the x-ray yields.

VII. DISCUSSION AND SUMMARY

The smallest cross section measured in this study is 0.1 mb and was done with only a one-hour-long bombardment. It appears to us that cross sections a factor three smaller could be measured by simply extending the length of the bombardment and increasing the beam intensity. Further increases in sensitivity could be obtained by studying the sources of background and taking steps to reduce them. In the case of $^{16}\text{O} + ^{154}\text{Sm}$, the $2n$ evaporation leads to a stable nucleus and thus a small correction would have to be applied for this unobserved yield at bombarding energies much below 60 MeV.

It does not appear possible for the moment to improve significantly on the precision of the method, since the largest source of error is currently associated with the absolute x-ray intensities. Computer-based calculations of the absolute intensity from the evaluated level schemes, which can be performed by the Nuclear Data Project at Oak Ridge National Laboratory, would be desirable in that they would both eliminate a lot of work and reduce the possibility of error in the evaluation of the absolute intensities from the level schemes. It might well turn out that we have overestimated the uncertainty on these values.

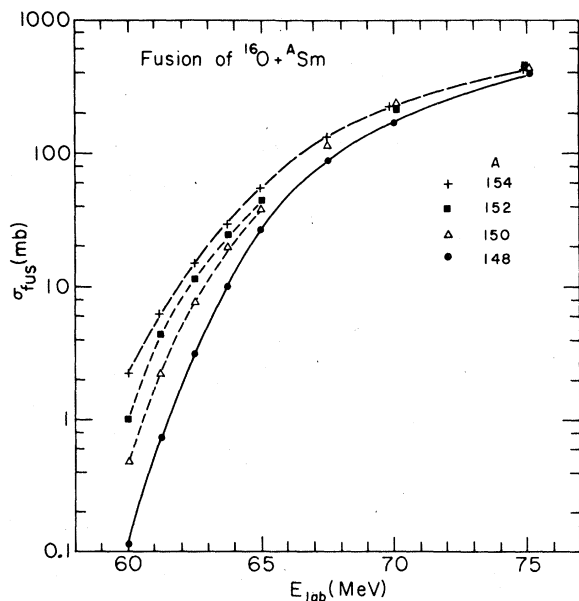


FIG. 7. The fusion cross sections as a function of bombarding energy. The total error on each point is $\pm 10\%$. The fusion cross sections, similar at energies well above the fusion barrier, vary markedly at low energies with the more deformed isotopes having the larger cross sections. The lines are to guide the eye.

The above errors on the fusion cross section do not include any contribution from the uncertainty in the beam energy. For 60 MeV $^{16}\text{O} + ^{148}\text{Sm}$, $(d\sigma/\sigma) \cdot 1/dE$ is $\sim 15\%$ per 100 keV. An uncertainty of $\pm 0.15\%$ in the beam energy thus results in a $\sim 15\%$ uncertainty in the cross section at this energy. However, this error on the beam energy is systematic and common to all bombardments.

Since the determination of the fusion cross section has been the goal of this study, a detailed statistical model analysis of the x - n distribution has not been undertaken. Some evaporation calculations¹⁶ confirmed our expectation that the systematic behavior shown in Fig. 6 is reasonable and that charged-particle emission is generally small. Nevertheless, a careful analysis of the results presented here would be worthwhile, especially since the prediction of the x - n distributions is rather sensitive to the strength of the γ -ray competition. The latter quantity is of current interest in predicting the γ -ray multiplicity. Thus, the present data might be useful in calibrating statistical model calculations.

In summary, fusion cross sections for the reaction of $^{16}\text{O} + ^{148,150,152,154}\text{Sm}$ have been measured by observing the delayed x rays from evaporation residues trapped in a catcher foil. This technique

has enabled the determination of cross sections as small as 0.1 mb to a precision of $\pm 10\%$. The yields of individual isotopes could be determined from an analysis of the time dependence of the x-ray yield. The principle source of error in this technique has been the absolute intensities of the x rays emitted by the radioactive evaporation residues and their daughter activities. The fusion cross sections were found to be similar at energies well above the fusion barrier, but to differ markedly at energies well below the barrier.

ACKNOWLEDGMENTS

We wish to thank B. Feldman, E. Skurnik, and L. Sapir and their staffs for assistance with some technical aspects of the experiments. The help of Dr. A. Gavron in performing the statistical model calculations is acknowledged. One of us (R.G.S.) would like to thank Professor Z. Fraenkel and Professor G. Goldring for the stimulating scientific atmosphere and friendly hospitality he enjoyed during his visit at the Weizmann Institute. This research was sponsored in part by the U. S. Department of Energy under Contract No. W-7405-eng-26 with Union Carbide Corporation.

¹L. C. Vaz and J. M. Alexander, Phys. Rev. C 10, 464 (1974).

²L. C. Vaz and J. M. Alexander, Phys. Rev. C 18, 2152 (1978).

³R. G. Stokstad, Y. Eisen, S. Kaplanis, D. Pelte, U. Smilansky, and I. Tserruya, Phys. Rev. Lett. 41, 465 (1978).

⁴D. L. Hendrie, N. K. Glendenning, B. G. Harvey, O. N. Jarvis, H. H. Duhm, J. Saudinos, and J. Mahoney, Phys. Lett. 26B, 127 (1968); N. K. Glendenning, D. L. Hendrie, and O. N. Jarvis, *ibid.* 26B, 131 (1968); W. Brückner, D. Husar, D. Pelte, K. Traxel, M. Samuel, and U. Smilansky, Nucl. Phys. A231, 159 (1974); A. H. Shaw and J. S. Greenberg, Phys. Rev. C 10, 263 (1974).

⁵T. Sikkeland, Phys. Rev. 135, B669 (1964).

⁶H. H. Gutbrod, W. G. Winn, and M. Blann, Nucl. Phys. A213, 267 (1973).

⁷F. Pühlhofer, W. Pfeffer, B. Kohlmeyer, and W. F. W. Schneider, Nucl. Phys. A244, 329 (1975).

⁸J. B. Natowitz, Phys. Rev. C 1, 623 (1970).

⁹R. Broda, M. Ishihara, B. Herskind, H. Oeschler, S. Ogaza, and H. Ryde, Nucl. Phys. A248, 356 (1975).

¹⁰Obtained from Seforad Applied Radiation, Ltd., Emek Hayarden, Israel.

¹¹R. A. Mowatt, Nucl. Instrum. Methods 70, 237 (1969).

¹²N. B. Gove and M. J. Martin, Nucl. Data Tables A10, 205 (1971).

¹³A. H. Wapstra, G. J. Nijgh, and R. Van Lieshout, *Nuclear Spectroscopy Tables* (North-Holland, Amsterdam, 1959).

¹⁴R. S. Hager and E. C. Seltzer, Nuclear Data Tables A4, 1 (1968).

¹⁵*Nuclear Data Sheets*, edited by W. B. Ewbank for the Nuclear Data Project (Academic, New York).

¹⁶Monte Carlo statistical model code JULIAN, M. Hillman and Y. Eyal (unpublished), as modified by A. Gavron.

¹⁷L. C. Northcliffe and R. F. Schilling, Nucl. Data Tables A7, 233 (1970).